NTNU – Trondheim
Norwegian University of
Science and Technology

Partial Discharge Measurements for Studying Cavities in Mass Impregnated Cables

Bjørn Helle Jørgensen

Master of Science in Electric Power Engineering
Submission date: June 2012
Supervisor: Magne Eystein Runde, ELKRAFT
Co-supervisor: Erling Ildstad, ELKRAFT

Norwegian University of Science and Technology
Department of Electric Power Engineering

Problem description

The electric insulation in HVDC subsea cables consists of paper impregnated with high viscosity oil (the “mass”). It turns out that differences in thermal expansion and contraction between the mass and the paper may cause cavities to form within the insulation during cool-down, leading to a dielectric breakdown. The cavities are essentially a result of an insufficient radial flow of the mass impregnation, and the power rating of such cables is largely set by considering this risk. However, the cavity formation process is not well understood.

SINTEF Energy Research and NTNU are contracted to study cavity formation during load cycling on a short length of the NorNed cable installed in the laboratory. It is assumed that cavities are associated with generation of partial discharges (pd) when voltage is applied across the insulation. Hence, cavity formation will be studied through measurement of pd activity, under various experimental conditions (thermal cycling, temperature level, external pressure etc).

The student project work is to take part in building an experimental setup for pd measurements on a short length of the NorNed cable in the laboratory, and to carry out preliminary measurements. This includes designing cable bushings and performing measurements at different cable temperatures and the interpretation of the results.

Preface

This work is part of a larger project which intends to use partial discharge measurements under AC stress as a means to map the characteristics of cavities within paper-mass insulation. AC is applied in order to be able of investigating PD activity at voltages well below the rated voltage of the test object. The repetition rate for discharges is also substantially higher under AC stress compared to DC stress making PD measurements easier. The project was initiated in 2011 and will continue through 2015. This work can be seen as a part of the start-up phase, familiarizing with the test objects and obtaining the suitable path for future work.

I would like to thank my supervisor Prof. Magne Runde and co-supervisor Prof. Erling Ildstad for guidance and fruitful discussions throughout the project. I would also like to thank H. Förster and O. Lillevik for advice and facilitating through the months of lab work.

Trondheim, June 2012

Bjørn Helle Jørgensen

Abstract

A hypothesis regarding temperature dependant discharge levels was the starting grounds for this student work. Based on calculations and conversations with experienced people in this field, there should be cavity-induced discharges at relatively low voltages when dealing with a paper-mass cable at room temperature.

PD measurements with a paper-mass HVDC cable under AC stress have been carried out. To get an understanding on the cavity characteristics at different temperature levels, the cable has been heated to temperatures of 20, 30, 40, 50 and 60°C.

Discharges over a large range of magnitude, from 10^1 to 10^4 pC was observed. The discharges measured coincide with rather large portions of a butt gap being drained of oil.

Partial discharges are a stochastic variable, thus one cannot expect values to coincide from measurement to measurement, but rather focus on finding tendencies. The maximum discharge levels showed a temperature dependency, but not as easily interpretable as expected. During the first half of the temperature cycles the maximum discharge levels varied as anticipated; small to non existing discharges at high temperatures and larger discharges at room temperature. This correlation became less clear over time. The deviation from the anticipated characteristics could be caused by:

- Temperature gradients over the insulation due to insufficient time to stabilize at the wanted temperature level.
- Axial oil flow in the test object.
- Irreversible deterioration of the insulation caused by large discharges mid-test.

The discharge characteristics did show two clear tendencies throughout the lab work:

- Whenever the temperature was raised from one level to a higher level, the maximum discharge size was reduced.
- The inception voltage increases with increasing temperature and decreases with decreasing temperature

The cable was installed in a test rig prior to start-up of the student project. Initially there was PD activity in one of the terminations which had to be modified to some extent to avoid interferences on the measurements. A new test object is under preparation and new terminations have been designed. The new terminations are based on the old design and the modifications made on it. Drawings for the new terminations have been made for the workshop and the fabrication process followed up. Measurements to locate the discharge sites were performed at room temperature at the end of the lab work. These measurements indicated an even distribution of the discharge sites along the length of the cable, meaning the terminations can be deemed healthy.

Sammendrag

En hypotese om temperaturavhengige utladningsnivåer var utgangspunktet for arbeidet utført i denne studentoppgaven. Basert på samtaler med erfarne personer innenfor dette fagfeltet samt egne beregninger, forventes hulromsutladninger i en masseimpregnert kabel ved romtemperatur.

En masseimpregnert HVDC kabel har blitt satt under AC-påkjenning og utladningsmålinger har blitt utført. For å undersøke sammenhengen mellom temperatur og utladningsnivå har målinger blitt utført på 20, 30, 40, 50 og 60˚C.

Utladningene som har blitt målt har vært i størrelsesordenen 10^1 til 10^4 pC. Størrelsesordnenen for utladningene stemmer overens med beregninger for tilsynelatende utladninger ved store hulrom i butt gap, størrelsen vil avhenge av hvor stor del av butt gapets areal som er gassfylt.

Partielle utladninger opptrer som en stokastisk variabel og samme resultat fra måling til måling kan ikke forventes. Sammenhenger i utladningkarakteristikken bør derfor vær fokus fremfor absolutte tallverdier. Den maksimale utladningstørrelsen viser en temperaturavhengighet, men ikke fullt så entydig som man håpet på i oppstarten av prosjektet. Under første del av målingene fulgte utladningsnivået det forutsette mønsteret med lite til ingen utladningsaktivitet ved høye temperaturer og større utladninger ved romtemperatur. Under etterfølgende målinger var ikke sammenhengen temperatur/utladningsnivå like tydelig. Avvikene fra den forventede oppførselen kan ha flere årsaker, for eksempel:

- Kabelen har ikke fått nok tid til å stabilisere seg på det ønskede temperaturnivået og temperaturgradienter er tilstede over isolasjonen.
- Aksiell oljevandring i testobjektet.
- Nedbryting av isolasjonen under store utladninger midtveis i testingen.

To tendenser var tydelige gjennom hele måleprosessen:

- Ved økning av temperaturen fra ett nivå til et høyere nivå, gikk maksimal utladningsstørrelse ned.
- Tennspenningen for utladninger øker ved økende temperatur of synker ved redusert temperatur.

Kabelen var montert i en rigg med hjemmelagede termineringer før studentarbeidet begynte. En av termineringene viste utladningsaktivitet som måtte gjøres noe med før måling på isolasjonen kunne startes. Termineringen ble utladningsfri etter noe ombygging og remontasje. Et nytt testobjekt er under forberedelse og nye termineringer har blitt designet basert på det gamle testobjektet og endringene utført på dette. Tegninger til verkstedet har blitt laget og monteringsjobben fulgt opp underveis. Som en avsluttende labøvelse ble lokaliseringsmålinger utført for å finne utladningskildene. Lokaliseringsmålingene viste en jevn fordeling av utladningskilder langs kabelen, ikke fra endeavslutningene.

TABLE OF CONTENTS

1 INTRODUCTION

Paper-mass cables have been in use for more than 100 years. Previously this lapped insulation was used in medium voltage (MV) AC installations, but today it is only installed in DC transmissions. This insulation has proven to be a stable design and several older cables are still in operation. [1]

At the center of the cable lies the conductor with the conductor screen. The intent of applying the semiconducting screens, in this case carbon-black paper, is to provide a smooth transition between the paper-mass insulation and the lead sheath/conductor, avoiding local field enhancements.

The paper/mass insulation system of a typical mass-impregnated cable is shown in Figure 1.1. The paper strips are applied as open helixes, i.e, there are small gaps in the insulation. These gaps are referred to as butt gaps. The reason for lapping in open helixes as opposed to closed helixes is to make the cable somewhat flexible. When the insulation system has been lapped onto the conductor, the core is vacuum-heat-dried to remove water trapped within the paper and then impregnated with high viscosity oil.

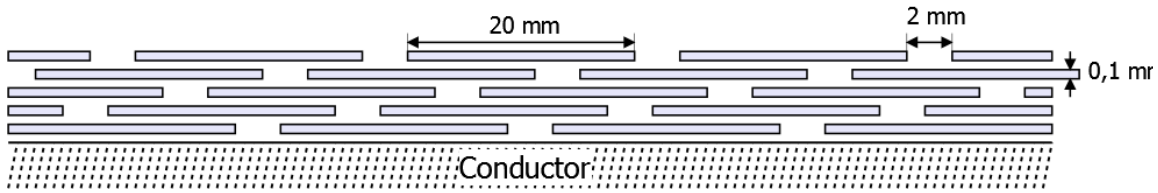

Figure 1.1 - Paper-mass insulation system. Inner semiconductor not included.

After the impregnation process the core is sealed with a lead sheath. The lead sheaths task is to prevent water from penetrating into the paper/mass insulation, whilst also keeping the mass from leaking to the surroundings. The lead sheath is protected from corrosion and mechanical wear during production by means of a polymeric layer extruded directly onto the lead. As the lead is inelastic and do not supply any real mechanical strength, there is a steel sheath lapped onto the polymeric layer to keep the insulation system in its place.

1.1 Field distribution in HVDC cables

AC/Transient state:

As voltage is applied to the cable, the electric field distribution is governed by the permittivities of the materials. The relative permittivity, ε_r, of mass-impregnated paper is approximately 4 and the relative permittivity of the mass itself is approximately 2 [3]. Assuming there are no charges present at the interfaces, the flux density must be constant. Thus:

$$D_m = D_p \tag{1}$$

then

$$\varepsilon_0 \varepsilon_m E_m = \varepsilon_0 \varepsilon_p E_p \rightarrow E_m = \frac{\varepsilon_p}{\varepsilon_m} E_p \quad (2)$$

This implies that as the voltage is turned on and in AC application, most of the electric field will be over the mass filled areas between the papers.

DC/static state:

Assume uniform current density:

$$j_p = j_m \quad (3)$$

then

$$E_p \sigma_p = E_m \sigma_m \rightarrow E_p = \frac{\sigma_m}{\sigma_p} E_m \quad (4)$$

When the voltage has been applied for some time (static state), the field distribution is governed by the conductivities of the materials. The electric stress in the insulation will therefore gradually shift to the paper, which has the lowest conductivity.

Considering the insulation as a cylinder capacitor, the field distribution is expressed by formula 5. U being the applied voltage over the insulation, r_o and r_i the outer and inner radius of the insulation respectively. [2]

$$E(r) = \frac{U}{r ln \frac{r_o}{r_i}} \quad (5)$$

From this expression the graph displayed in Figure 1.2 can be drawn and the field enhancement factor calculated. For this cable the field enhancement factor ($E_{max}/E_{min} = r_0/r_i$) is 2,2. This graph is based on the actual dimensions of the test objects to be examined in this project.

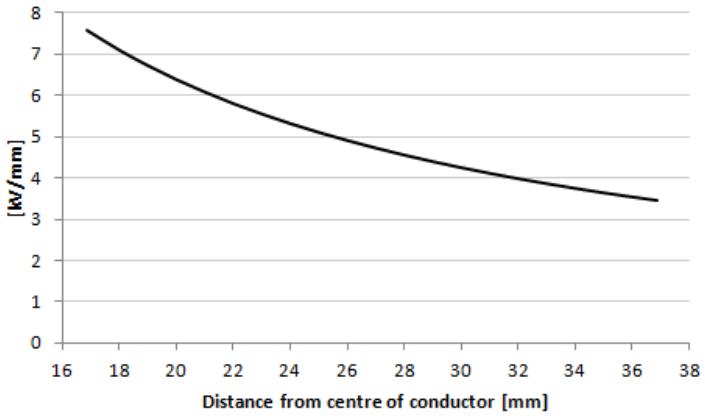

Figure 1.2 - Voltage distribution over the insulation with 100 kV applied to the cable.

1.2 Formation of cavities

Research has showed that cavities in this type of insulation typically starts in the butt gaps and continue between the paper layers towards adjacent butt gaps. [3] In a mass-impregnated cable, the oil constitutes approximately 40% [9] of the insulations volume whilst the butt gap/paper ratio is normally somewhere around 1/10. Assuming the insulation is cavity free at 50-55℃ [4] and stored at room temperature (20℃) some calculations can be done:

$$\Delta V_{oil} = V_0 \beta \Delta T = 6{,}4 * 10^{-4}(55 - 20) * 0{,}4V_0 = 0{,}009V_0 \qquad (6)$$

Hence, the oil will contract by 9‰ of the total volume. Assuming the paper is not contracting and the oil only draining butt gaps, this could be sufficient to drain approximately 9/100 of the total butt gap volume of a cable.

1.3 Scope of work

As the oils thermal expansion coefficient is significantly larger than the coefficient of paper, cavities are expected to be formed when the cable temperature gets below the saturated temperature, 50-55℃. The calculations in 1.2 imply that if the cable is at room temperature, cavities are expected to be present. These cavities present at room temperature should be reduced both in size and quantity if the cable were to be heated. As shown in 2.2.3, the size of the discharge is proportional to the size of the cavity, thus a correlation should be observable by PD (partial discharge) measurements.

In order to perform PD measurements on the cable insulation, discharge-free HV terminations have to be in place. Initial problems with the first design have been sorted out, and a new design for future test objects has been developed.

2 PARTIAL DISCHARGES (PD)

2.1 Characteristics of PDs

During the lab work two "groups" of PD activities have to be taken into consideration. The first one, PDs in cavities, is the ones expected to appear within the cable. The other, corona discharges, also have to be kept in mind as they will act as noise in the measurements and should be avoided. Corona discharges can also occur within the cable, but it is more likely that they occur in a laboratory with limited space around the test object.

2.1.1 PDs in cavities

If a gas filled cavity is present within a solid insulation material, the abc-equivalent, shown in Figure 2.1, is a useful tool for understanding what is going in the test object.

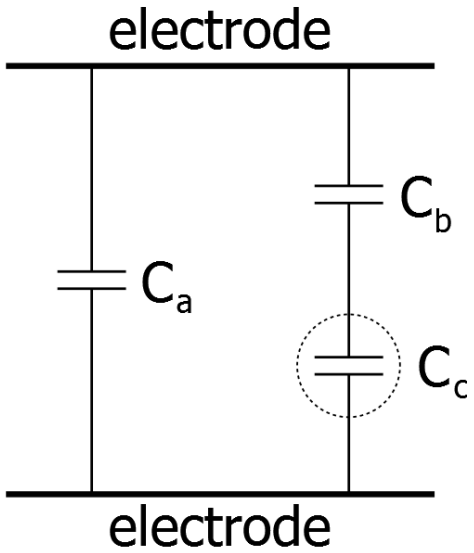

Figure 2.1 – abc-equivalent. Ca represents the capacitance of the healthy insulation between the two electrodes. Cb represents the capacitance between the edges of the cavity and the electrodes. Cc represents the capacitance of the cavity itself. Normally Cb<Cc<<Ca [2]

The voltage over the cavity, U_c, without discharges will follow the applied voltage U by capacitive voltage division according to Formula 7, in which C_a, C_b and C_c denotes the capacitances in the abc-equivalent.

$$U_c = U\frac{C_b}{C_b + C_c} \tag{7}$$

If the voltage U_c becomes greater than the electric breakdown strength of the cavity discharges will occur. The breakdown strength of the cavity will depend both on the geometry of the cavity and the Paschen curve of the gas within the cavity. PDs in cavities normally appear at the steepest parts of the voltage sinus, as shown in Figure 2.2. [3] As can be seen from this figure, the discharges continue prior to zero crossing of the applied voltage. This is because during the discharge, charge is moved from one wall of the cavity to the opposite

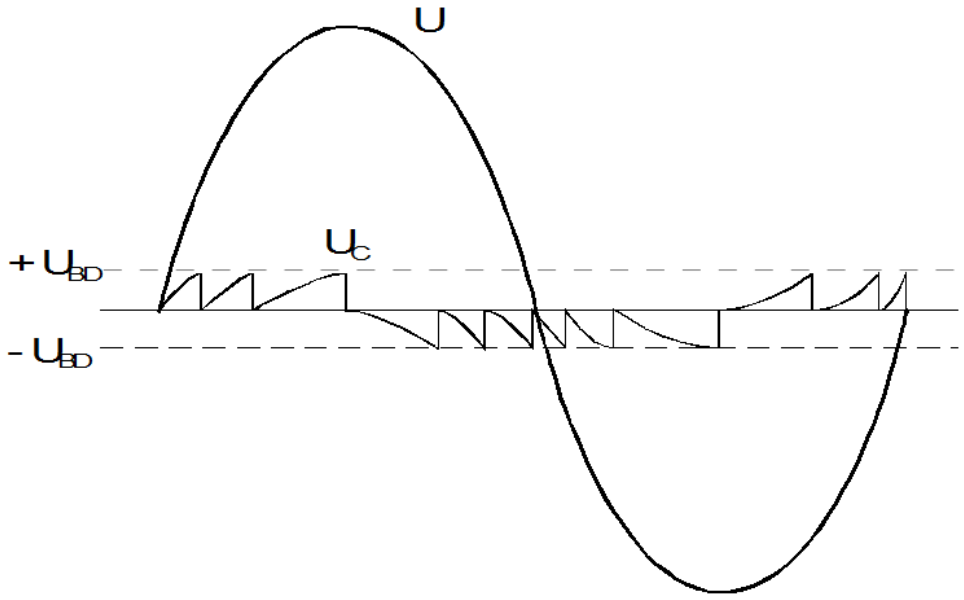

Figure 2.2 – The voltage over the cavity with discharges. U: applied voltage, Uc: voltage over the cavity, UBD: breakdown voltage of the cavity. [3]

wall, causing a potential offset across the cavity. The voltage across the cavity is still linked to the applied voltage by capacitive coupling, meaning it can reach $-U_{BD}$ while the applied voltage still is positive but with a negative du/dt. [3]

2.1.2 Corona discharges

Corona discharges typically occur if there are sharp points on an electrode in an insulating system. A sharp point on the earthed side will give a discharge in the positive half period of the applied voltage, whilst a sharp point on the high voltage (HV) side will give a discharge in the negative half period. This characteristic is used to check the phase of the applied voltage relative to the reference voltage (Figure 2.3).

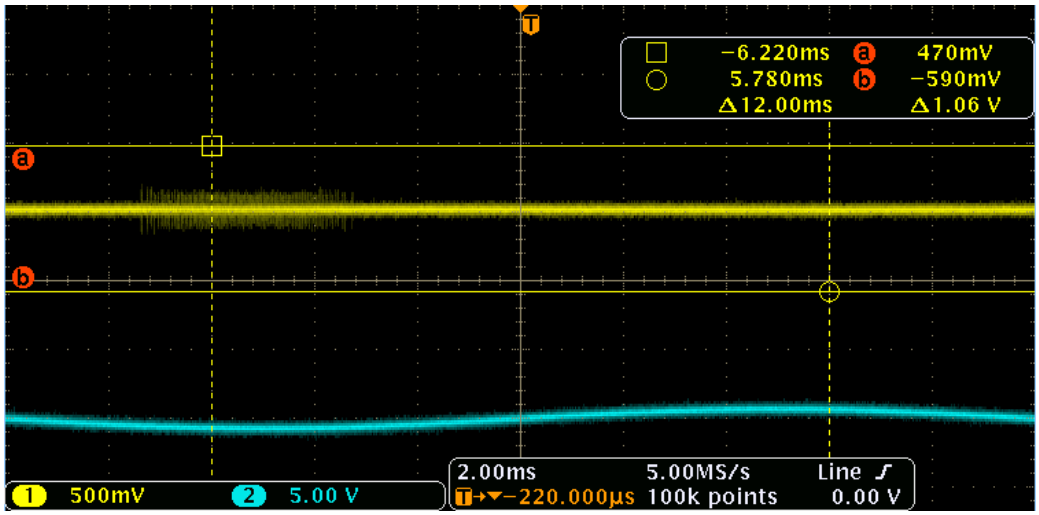

Figure 2.3 – Checking the phase of the reference voltage by attaching a wire to the HV conductor to initiate corona discharges.

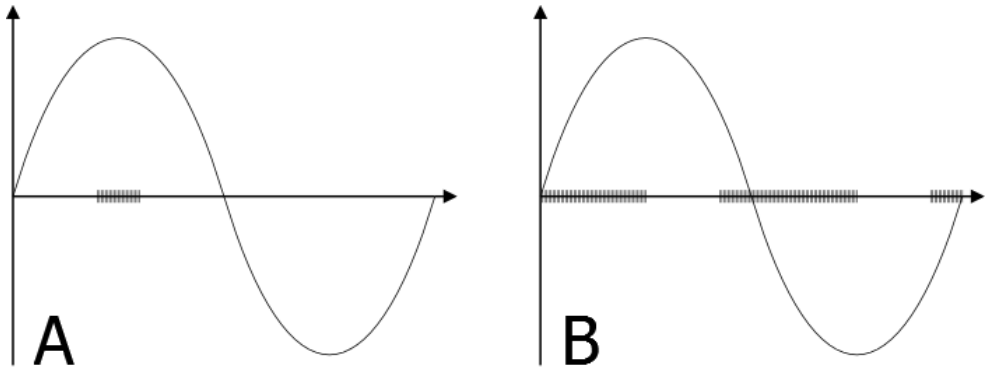

Figure 2.4 – Comparison of typical oscilloscope outputs with corona discharges (A) and cavity discharges (B). The corona discharges in "screenshot" A corresponds to a sharp point on the earthed side of the insulation system.

Corona discharges typically occur at and around the voltage peaks. Exterior corona discharges are avoided using corona-rings and other electrical shielding such as metal sheets to cover pointy surfaces and to ensure a homogeneous electric field. Exterior corona can be located using a corona gun to locate the discharge site. This has been done continuously throughout the lab work to ensure no exterior interferences on the measurements. The easiest way to separate corona discharges from cavity discharges is to examine the time at which they occur, like in the illustrations of typical oscilloscope readings in Figure 2.4.

2.2 PD measurements

2.2.1 Measurement principle

A simplified setup used for PD-measurements is shown in Figure 2.5. A discharge in the test object will cause a lack of charge over the assumed cavity within the insulation, causing a transient voltage dip over the test object. This lack of charge is taken from the coupling capacitor, C_k, causing a small current to flow. This current flows through the measuring impedance, Z_m, and is picked up by the scope as a voltage pulse.

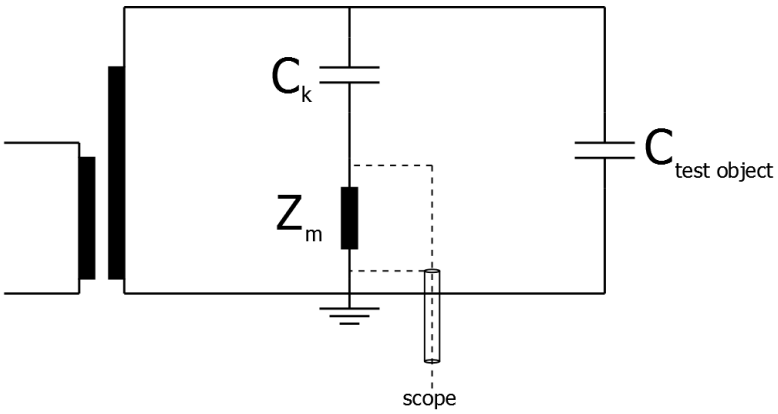

Figure 2.5 - Test circuit for PD-measurements. Ck: Coupling capacitance, Zm: Measuring impedance.

2.2.2 PD site localization

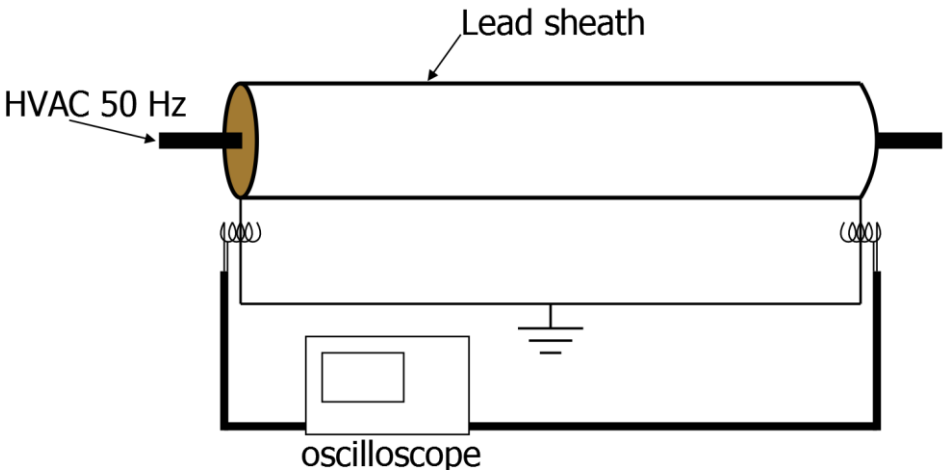

Figure 2.6 – Localization by measurements of wave propagation time. The discharge pulse will be picked up at both ends and the location can be calculated based on the time difference.

To locate the discharge sites the circuit shown in Figure 2.6 can be used. Initially a calibrator was connected to one side of the cable to determine the travel time for the whole cable, which turned out to be 34 ns (appendix V). The distance from the first side to pick up the discharge pulse to the discharge site, d, can be expressed as:

$$d = \frac{L - v\Delta t}{2} \tag{8}$$

In which L is the total length of the cable, v is the wave speed and Δt is the time difference between the pulses.

2.2.3 Apparent charge

The previously mentioned research of Evenset [3] showed that cavities within lapped insulation generally start in the butt gaps. The approximate size of expected discharges, in terms of coulombs, and the apparent charge measureable can be calculated like shown in the example below.

Assume an air-filled cavity in a butt gap, 2,5 mm (width of a typical butt gap) by 2,5 mm and 0,1 mm high(typical paper thickness) => A=6,25 mm^2, d=0,1 mm. The previously mentioned abc-equivalent is applied.

The capacitances of the abc-equivalent are calculated:

$$C_a = \frac{\varepsilon_0 \varepsilon_r 2\pi l}{ln\frac{r_o}{r_i}} = \frac{8{,}85 * 10^{-12} * 4{,}6 * 2\pi * 6}{\ln \frac{36{,}85}{16{,}85}} = 2\ nF \tag{9}$$

The capacitance C_a has also been measured at 2nF using a capacitance meter.

$$C_b = \frac{\varepsilon_0 \varepsilon_r A}{d} = \frac{8{,}85 * 10^{-12} * 4{,}6 * 6{,}25 * 10^{-6}}{20 * 10^{-3}} = 0{,}013\ pF \quad (10)$$

$$C_c = \frac{\varepsilon_0 A}{d} = \frac{8{,}85 * 10^{-12} * 6{,}25 * 10^{-6}}{0{,}1 * 10^{-3}} = 0{,}553\ pF \quad (11)$$

According to the Paschen curve for air, the breakdown voltage, U_{BD}, assuming 1 atm pressure within the cavity, is approximately 500 V. In formula 12 ΔU_c is the voltage change over the cavity during discharge whilst U_{rem} is the remnant voltage over the cavity after the discharge. The remnant voltage will depend on both the conductivity of the insulating material and the surfaces of the cavity.

$$\Delta U_c = U_{BD} - U_{rem} \quad (12)$$

Assume U_{rem}=0 to make calculations possible => ΔU_c=500 V. The size of the discharge within the insulation, q_i is calculated:

$$q_i = \Delta U_c C_c = 500\ V * 0{,}553\ pF = 267\ pC \quad (13)$$

This discharge cannot be measured on the external circuit. During the discharge the charge transfer across the cavity can be thought of like an injection of charge over C_c. Assuming no current flows in the external circuit, the equivalent circuit will then be like Figure 2.7.

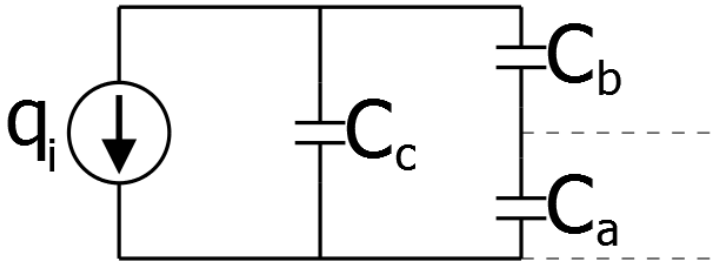

Figure 2.7 – abc-equivalent during discharge [2]

The discharge which can be measured externally will correspond to the charge injection according to formula 14. This is the apparent charge that gives an indication regarding the needed sensitivity and the magnitude of the expected discharges to be measured.

$$q_s = q_a = \Delta U_a C_a = \Delta U_c \frac{C_b}{C_a} C_a = \Delta U_c C_b = 6{,}5\ pC \quad (14)$$

This magnitude of q_i is merely an approximation because:

- The remnant voltage is unknown
- The pressure of- and the gas dissipated within the cavity is unknown, i.e. the Paschen curve is unknown

3 TEST SETUP

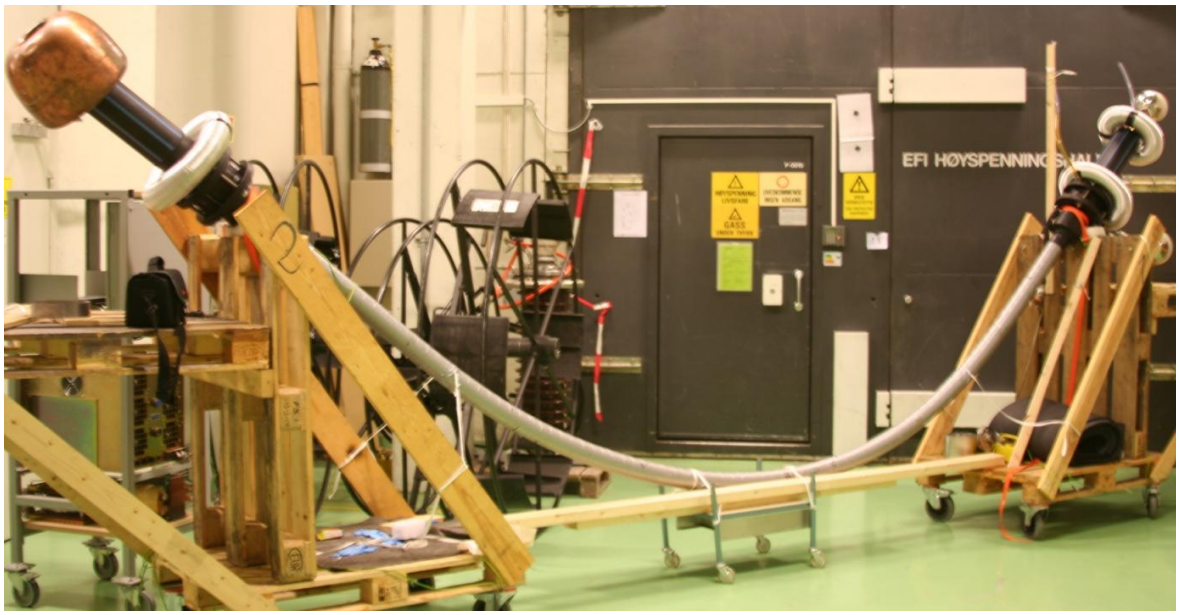

Figure 3.1 – Test object mounted on rig.

The test object, depicted in Figure 3.1, is an approximately 6m piece of the NorNed cable, stripped from armor and protective layers down to the steel sheath. This is a cut-off from the dual-core section of the NorNed cable, but with only one insulation system it is like any other HVDC cable.

The cable has been fitted with custom made terminations (described in chapter 4) as AC is applied to a DC cable and there are no factory-made terminations available. In addition to the connector on the main conductor, conductors are connected to both ends of the lead sheath to facilitate for proper grounding and the possibility of heating by passing current through the lead. The steel sheath has been kept in place to ensure mechanical strength and to prevent plastic deformation of the lead sheath during thermal cycling. The layers of the test object are described in Figure 3.2. Keep in mind that this is not the complete subsea cable.

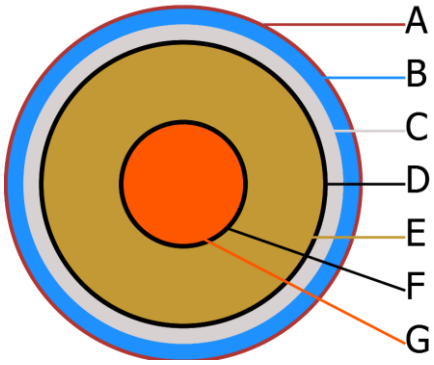

Figure 3.2 – Cross section illustration of the test object

Table 3.1 – Explanation to Figure 3.2.

Layer	Description	Thickness [mm]	Outer diameter [mm]
A	Steel sheath	0,55	89,7
B	PE layer	3,8	88,6
C	Lead sheath	3,1	81,1
D	Outer semiconductor (carbon black paper) and Hochstädter ribbon (perforated aluminum)	0,59	74,9
E	Paper-mass insulation	20	73,7
F	Inner semiconductor (carbon black paper)	0,48	33,7
G	Conductor (790 mm^2 Cu)	-	32,7

The measurement circuit used in most of the lab work (equipment set 1, appendix III) is shown in Figure 3.3. Due to current limitations in the control desk the circuit is compensated by two shunt reactors.

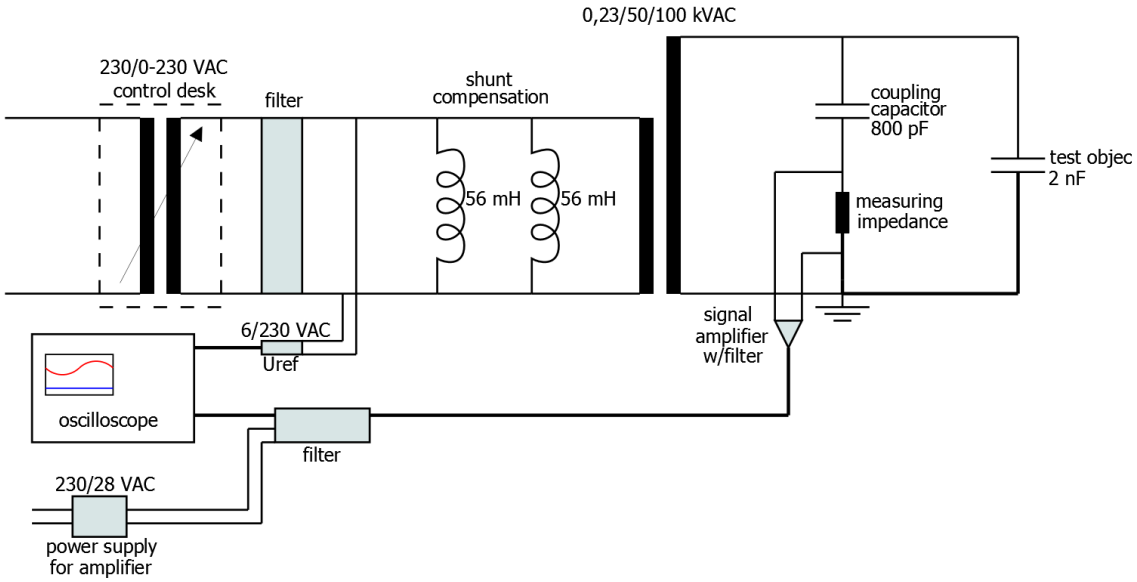

Figure 3.3 – Test circuit used in most the lab work.

Prior to performing measurements the circuit has to be calibrated, injecting a known charge over the test object and reading the oscilloscope output. The output will not be entirely proportional relative to the calibration pulse as the order of magnitude increases. This is because the capacitance of the calibrator increases when increasing the injected charge. This phenomenon is shown in Table 3.2. For oscilloscope screenshots see Appendix I.

Table 3.2 – Calibration pulses without signal amplifier

Injected charge [pC]	Output [mV]	Calibration [pC/mV]
100	6,7	14,9
1 000	62	16,1
10 000	510	19,6

4 CABLE TERMINATIONS FOR LAB USE

4.1 Introduction

When a high voltage cable is to be terminated, some sort of field control is necessary in order to avoid discharges and breakdown at the connection points. In an AC case the electric field is controlled by applying materials with a suitable shape and permittivity. Several methods for controlling the electric field are applicable, but an oil filled termination with field control rings of aluminum was initially chosen for this project. The reason for having oil filled terminations raised approximately 2 meters off the floor were to prevent axial flow of mass in the cable [4] and to achieve a high breakdown voltage with limited space, as opposed to air insulation.

4.2 First design

The first terminations were designed as shown in Figure 4.1. No field controlling materials such as stress cones or semiconducting materials were used in the first design; the field was simply rounded off at the transitions between lead sheath/ insulation and HV-connector/insulation by means of aluminum rings. The critical area in this design is the area surrounding the field control ring at ground potential. In this area the distance between high voltage potential and ground is the shortest, additionally this is where the outer semiconductor and Hochstädter ribbon is cut, with the risk of leaving fringed edges. Fringed edges could cause air bubbles to get stuck causing local field enhancements and/or make the electric field inhomogeneous.

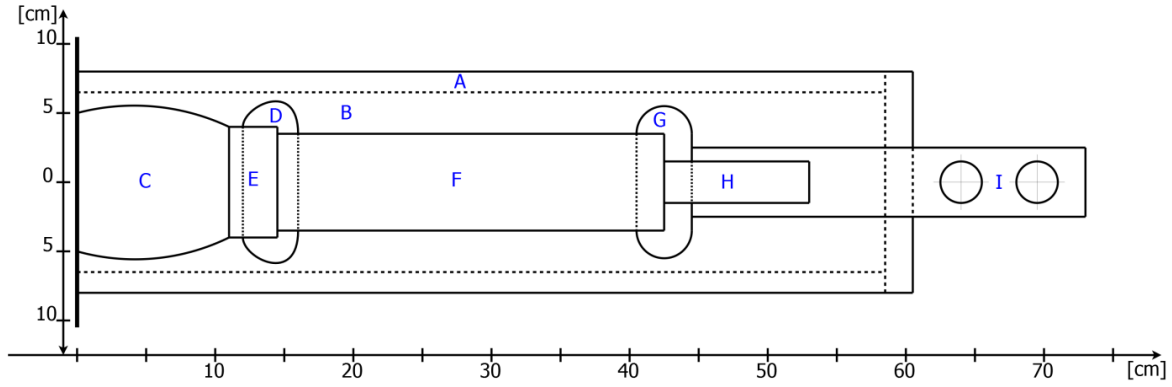

Figure 4.1 – The first cable termination design. A: PE body, B: Oil filled volume, C: Mechanical support, D: Al field control ring at ground potential, E: Lead sheath, F: Insulation stripped of outer semiconductor and Hochstädter ribbon, G: Al field control ring at HV potential, H: Conductor, I: Brass connector. Valves at top and bottom are not included in this illustration.

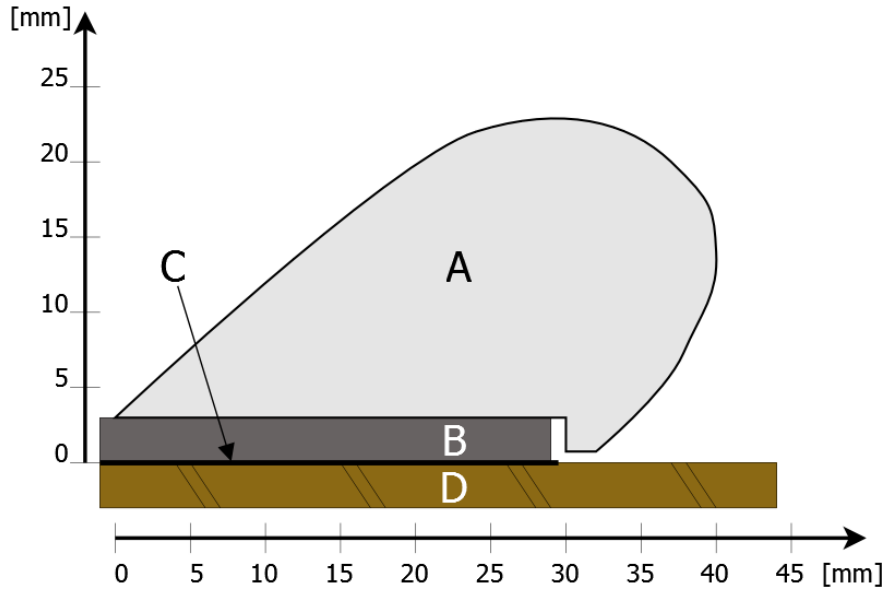

Figure 4.2 – Detailed view of the ground potential field control ring. A: Al-ring, B: Lead sheath, C: Outer semiconductor and Hochstädter ribbon, D: Paper-mass insulation.

A detailed illustration of the area surrounding the grounded field control ring is shown in Figure 4.2. If an air bubble was to be trapped in the gap between the aluminum ring, A, and the insulation, D, this would be worst case scenario as this is a high field area.

4.2.1 Measurements made with the first design

Measurements with the first design showed PD activity in one of the terminations, rendering measurements on the cable insulation impossible. Oscilloscope screenshots from one series of measurements are shown in appendix II. The characteristics of the discharge activity for the larger discharges correspond to the textbook example of discharges in cavities regarding PD inception- and extinction voltage. The expected discharge characteristic for cavities is shown in Figure 4.3.

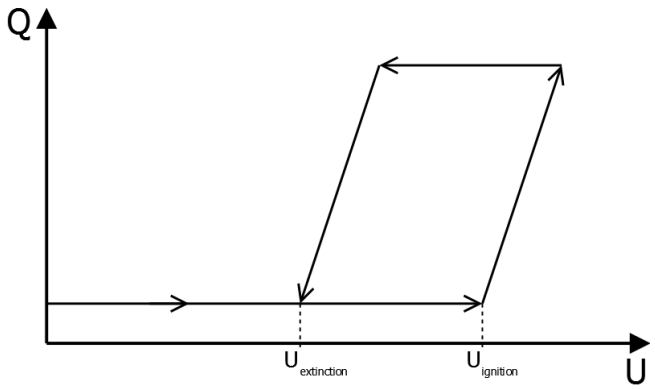

Figure 4.3 - Discharge characteristics with a cavity within solid insulation. The PD inception voltage for cavities is substantially higher than the extinction voltage due to charge conservation at the cavity's interfaces.

Initially locating the discharge site with acoustic sensors attached to the outside of the terminations was attempted, but nothing was detectable. Why the acoustic sensors could not pick up anything from the outside is not evident, but the cable mass may absorb the discharge pulses, making them hard to detect externally. The faulty termination was located using high frequency measurements, measuring the propagation time of discharge pulses from the discharge site to the two terminations

The faulty termination was drained of oil, cleaned and refilled. After the refill evacuation of air by means of a vacuum pump was attempted, but the stream of air bubbles had no end and seemingly came from a leak in the termination. Measurements were attempted after the reassembly but once again discharges occurred in the termination.

4.2.2 Modifications made on the first design

To reduce the risk of trapped bubbles and fringed edges, changes were made to the area surrounding the earthed Al-ring on the trouble-ridden termination. Further actions to make the termination leak free were also done. The modified design of the critical area surrounding the earthed Al-ring is shown in Figure 4.4.

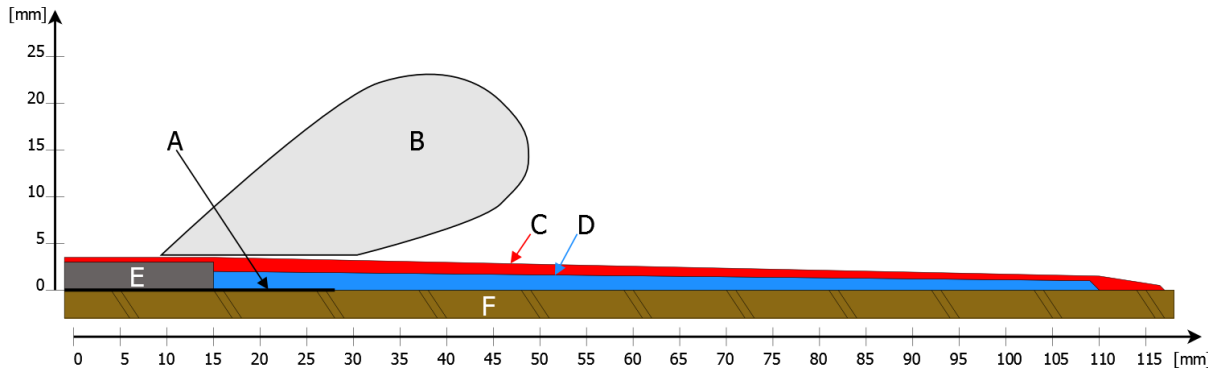

Figure 4.4 – Modified design on termination #2. A: Outer semiconductor and Hochstädter ribbon, B: Al-ring, C: Silicone tape, D: Stress controlling tape, E: Lead sheath, F: paper-mass insulation. The Al ring is connected to the lead by means of Cu strips.

In order to have control of the edges of the outer semiconductor and the Hochstädter ribbon, an additional 1,5 cm of lead was removed and the edges of the outer semiconductor was trimmed . Stress controlling tape was lapped from the lead sheath and outwards as a means of covering any fringed edges and to round off the electric field. Insulating silicone tape was lapped onto the stress controlling tape to ensure mechanical strength. The stress controlling tape has very nonlinear characteristics with an approximate equivalent circuit as shown in Figure 4.5. [6] As can be seen from this figure, the voltage distribution is frequency dependant, but this is more relevant when dealing with switching pulses. The field dependant resistive capabilities of the stress controlling tape are not utilized to a large extent in this termination. Sharp edges from the outer semiconductor and the Hochstädter ribbon will however be “electrically rounded off”.

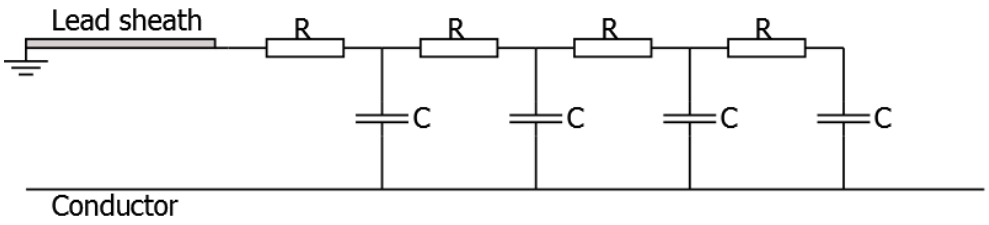

Figure 4.5 – Approximate circuit model for the stress controlling tape.

Comsol Multiphysics simulations have been carried out for both the modified and original designs of the terminations. Plots of both the old and the new configuration with equipotential lines are displayed in Figure 4.6. The characteristics of the stress controlling tape apart from high permittivity (25-30) [7] are not implemented in the simulations, but the plots give an indication of how the electric field will distribute.

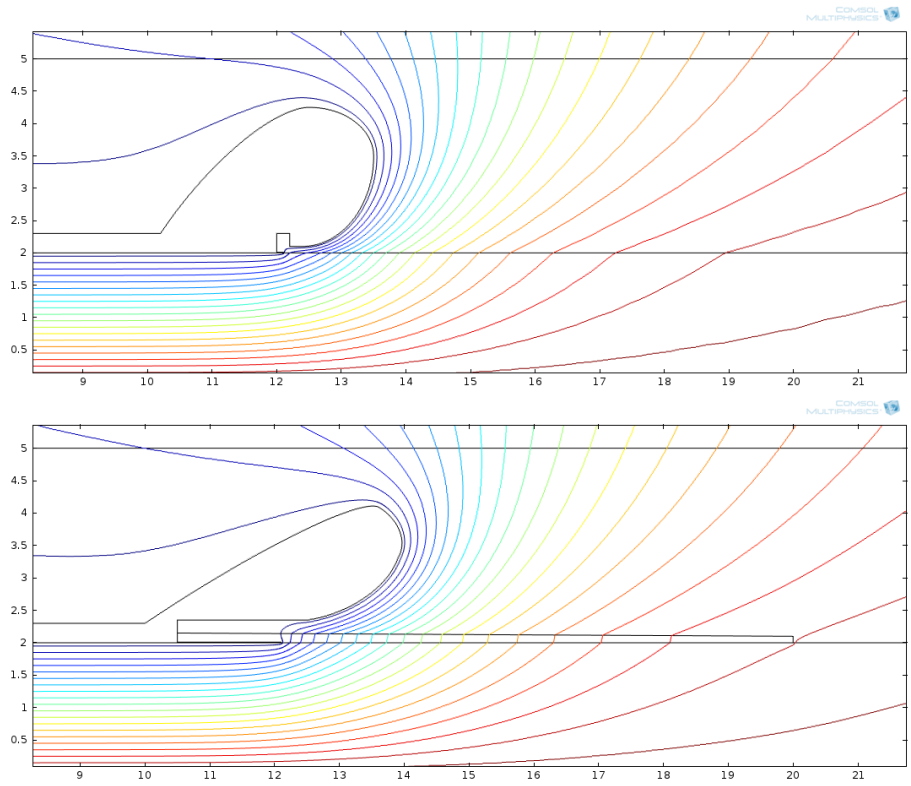

Figure 4.6 – Plots of equipotential lines by the earthed Al-ring. Top plot: Unmodified termination. Bottom plot: Modified termination with 1,5 cm of the lead sheath removed and 9,5 cm field controlling tape lapped onto the Hochstädter ribbon and further onto the insulation. Additionally the Al-ring has been modified to some extent. The Al-rings are not entirely correctly drawn, but the area of the rings facing the insulation (right) is rather precisely depicted.

4.3 Second design

Due to the problems experienced with the first design, changes were made in the preparation of the next test object. The new terminations have the same basic design as the first terminations, but the highly viscous mass in the terminations will be replaced by less viscous transformer oil in order to ease evacuation of air and speed to up the filling/draining processes. Silicone tape will be lapped further onto the insulation in order to separate the cable mass from the transformer oil. The modifications made on the first design regarding termination of the lead sheath and the outer semiconducting layers will be applied to the new design (Figure 4.4). Additional measures to keep the terminations leak free have also been made by replacing all flat gaskets with o-rings. The new design is shown in Figure 4.7.

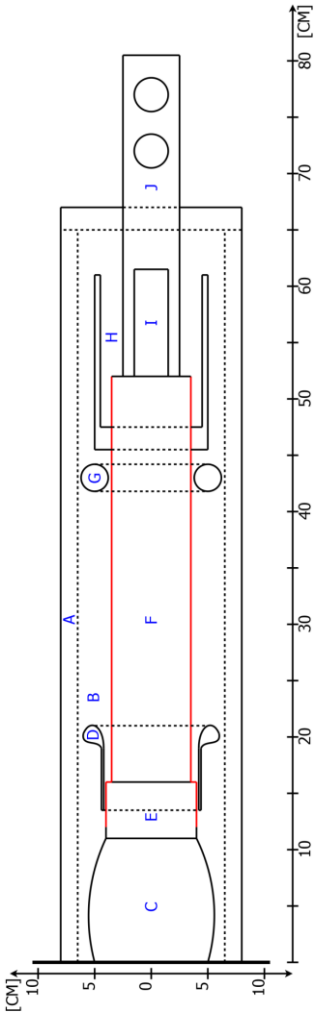

Figure 4.7 – New termination design, intended for close to vertical mounting. A: PE body, B: Oil filled volume, C: Mechanical support, D: Field control ring at ground potential, E: Lead sheath, F: Insulation stripped of outer semiconductor and Hochstädter ribbon, G: Field control ring at HV potential, H: Reservoir for cable mass, I: Conductor, J: Brass connector. The red lines indicate the silicone tape applied to separate the cable mass from the transformer oil. Valves at the top and bottom of the body are not shown in this figure.

The intent of the reservoir for cable mass is to provide overpressure to avoid axial oil travel. The reservoir is in the HV region, shielded by the field control ring, G, and can therefore be made of any material, conductive or not. One solution could be to make it out of metal and attach it to a flange with o-rings pressing towards the silicone tape, mechanically securing it by screws to the brass connector pressing from three sides. By placing the reservoir at HV potential the connection and securing of the field control ring could simply be done with Cu strips from the reservoir. Another alternative could be to make the reservoir partly or completely out of shrink hose, letting the deformation of the shrink hose supply the mechanical support.

During heating the paper and oil will expand relative to the lead sheath due to substantially higher thermal expansion coefficients. If one disregard friction and considers the paper and the oil filled butt gaps as a strip comprising of 1/10 butt gaps and 9/10 paper the expansion can be approximated as shown below:

$$\Delta l = l_0 \alpha \Delta T = 6\left(\frac{1}{10} * 2{,}13 * 10^{-4} + \frac{9}{10} * 13{,}4 * 10^{-6}\right) * 35 = 7\ mm \qquad (15)$$

This expansion would probably distribute evenly between the two sides, meaning a maximum displacement relative to the lead sheath of 3,5 mm. To take the thermal expansion into consideration and ease the fitting of the termination, the inner field control ring has been lengthened to the dimensions shown in detail in Figure 4.8.

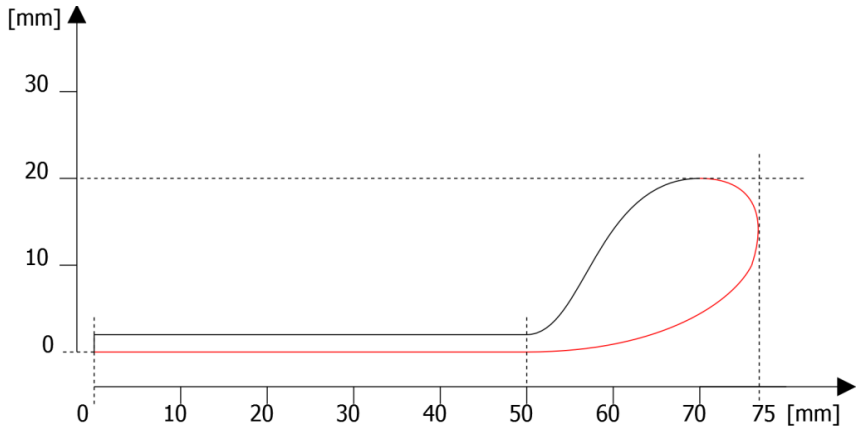

Figure 4.8 – Profile drawing for the inner field control ring as given to the workshop. The red lines indicate the critical area considering smoothness and shape. This field control ring will consist of a 50 mm long metal pipe with an inner diameter of 85mm and a lathe-made aluminum ring at the end facing the HV side.

5 RESULTS AND DISCUSSION

Partial discharges are stochastic variables and the reproducibility is very low for this kind of measurements. In this kind of work, one is looking for tendencies and correlations rather than expecting the output to be exactly like anticipated. All voltages are given as RMS values. The temperatures listed are not the exact values, the temperature was measured at two sites along the steel sheath and the listed temperature is the approximate mean value of the two measurements.

To check the quality of the modifications made on the first termination, the termination was fitted on the cable and tested. The testing was done by applying up to 25 kV without oil in the termination. No discharges were found with a sensitivity of 0,3 pC (measured in the EFI HV laboratory), and the termination was deemed healthy.

In order to investigate the correlation between cavities and temperature, the cable has been heated by passing current through the lead sheath and adding thermal insulation to the cable. The cable was heated to a maximum temperature of 60℃, as typical maximum continuous conductor temperature for mass cables is 65-70℃. [6] Heating was done from the outside and inwards to avoid temperature gradients within the insulation during measurements. All measurements from 10/5 and after were done in a laboratory with limited space. The limited space set an upper voltage limit of 70 kV due to problems with exterior corona at higher voltage levels. The equipment sets used in these experiments are listed in appendix III and some screenshots from the measurements are shown in appendix IV.

A summary of the highest measured discharges at the different voltage- and temperature levels are listed in Table 5.1. From this table a large span in magnitude of the discharges is observable, from 10^1 up to 10^4 pC. A precise calibration for the whole range is not possible, but the values give a good indication on the size of the discharges.

Table 5.1 – Summary of results. *: measurements done in the "EFI laboratory", a memory stick died and lab-notes were all remaining from that day. **Nothing was picked up without the amplifier so the amplifier was temporarily reconnected.

Eq. Set #	Date	T [°C]	q_{max} [pC]						
			10 kV	**20 kV**	**30 kV**	**40 kV**	**50 kV**	**60 kV**	**70 kV**
*	7/5	**20**	47 kV≈1 pC		60 kV≈1,7 pC		70 kV≈7 pC		
			after 25 min:		47 kV≈30 pC		60 kV≈320 pC	70 kV≈ ≥400 pC	
1	10/5	**60**	<2	8	17	17	35	29	
1	11/5	**60**	<2	<2	<2	<2	<2	3	<2
1	13/5	**20**	294	471	333	275	196	196	216
1	18/5	**20**	353	647	627	549	471	392	235
1	19/5	**50**	<2	<2	<2	4	4	7	9
1	20/5	**40**	<2	784	≥1 765	≥1 765	≥1 765	≥1 765	≥1 765
2	22/5	**40**	<100	<100	1 600	4 800	8 500	8 600	8 500
2/1**	23/5	**50**	<100	<100	<100	<100	<100	<100	14
2	25/5	**30**	1 200	4 400	3 100	6 100	5 600	-	5 200
2	26/5	**23**	4 500	9 400	3 600	3 100	2 500	1 800	1 500
2	28/5	**50**	<100	<100	1 300	3 000	4 300	4 300	4 300

5.1 Discharge sizes at various temperature levels

To ease the interpretation of the results listed in Table 5.1, the results have also been plotted in the chart shown in Figure 5.1.

During the first temperature cycles (20→60→20→50˚C) the discharge behavior are as anticipated; small to non existing discharges at high temperatures, and some discharges at room temperature. This corresponds to the theory of cavity formation at temperatures below 50-60˚C and an oil-saturated and more or less discharge free cable at the higher temperature levels. Remembering the calculations in 2.2.3, these discharges could stem from cavities in butt gaps based on their size, although with a much larger area of the butt gaps than used in the calculations.

If the cavities have grown into the oil film between the paper layers, like described in Eventset's research, this could also give larger discharges due to the reduced height of the cavity which could increase the breakdown voltage based on the Paschen curve. This is discussed in chapter 5.2.

During the subsequent temperature cycles (40→50→30→23→50˚C), the discharge levels deviate from the anticipated pattern.

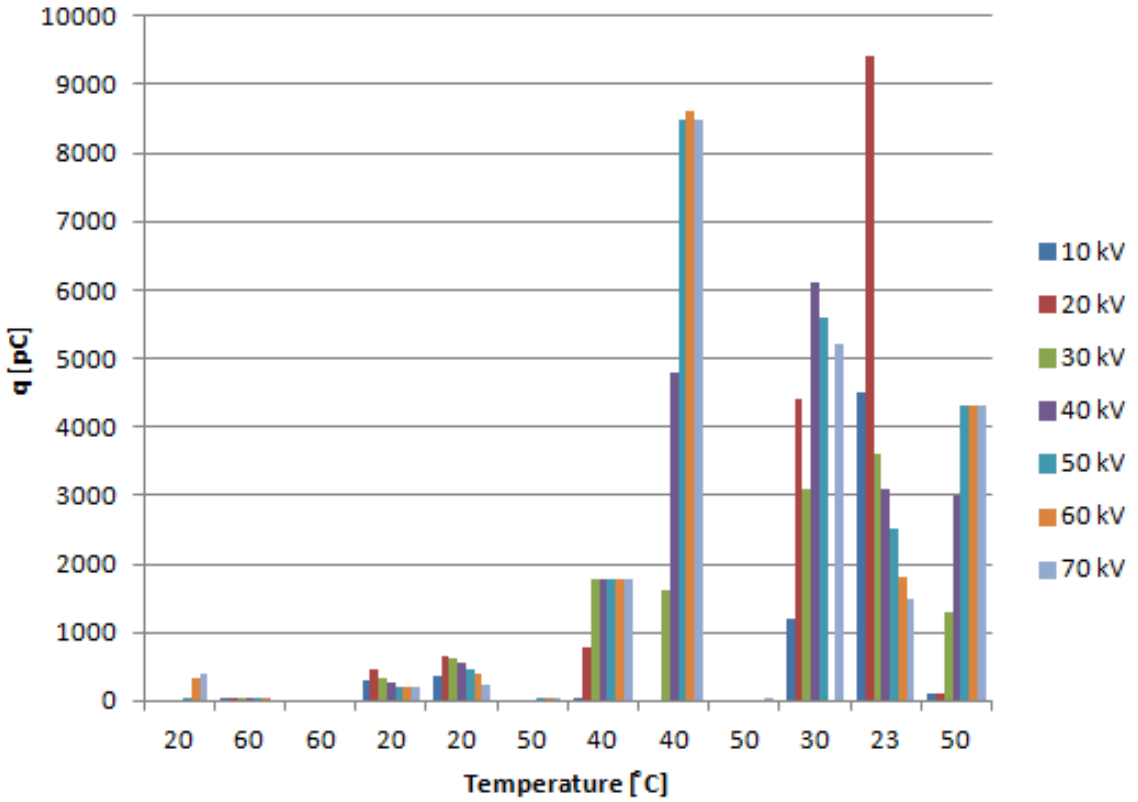

Figure 5.1 – Maximum discharge levels at the different voltages and temperatures. The temperatures are listed chronologically from left to right on the x-axis. All values ≤X has been set to zero in this chart. Please note that the columns of the first set at 40℃ are chopped and the amplifier removed at the subsequent measurements.

The large difference in temperature/discharge magnitude- response could have several causes, some of which are listed below:

- A remaining temperature gradient within the insulation, generally accepted as a cause for cavities in lapped insulation.
- Axial oil flow changing the internal oil distribution. (discussed in 5.4)
- The large discharges at 40℃ could have deteriorated the insulation to an extent which became evident once the temperature again got below 50℃. This is unlikely as this insulation, according to experts, is capable of withstanding very large discharges without deterioration.

Studying these results, one trend is consistent throughout the temperature cycles; the maximum discharge level decreases when increasing the temperature.

The first measurement series, including the first measurements at 40˚C was done with the signal amplifier connected and the subsequent series without the amplifier. There are large differences in the magnitude of the discharges prior to the two measurements at 40℃ and

after. The fact that the oscilloscope reached maximum input value prior to the change and once again measures ≈0 at 50℃ after the change makes the results trustworthy. Although this amplifier has been used in combination with the 300 kHz shunt earlier, there is probably no need for the signal amplifier in the work to come. This is because the discharges to be investigated appear to be of a magnitude of which the amplifier is unnecessary and this insecurity can be removed.

5.2 PD inception voltages

The PD inception voltage at the different temperature levels are shown in Figure 5.2. The inception voltages are not accurate values, but rather the first of the predetermined voltage levels at which discharges were observed. This is due to problems having control with both the applied voltage and the oscilloscope at the same time.

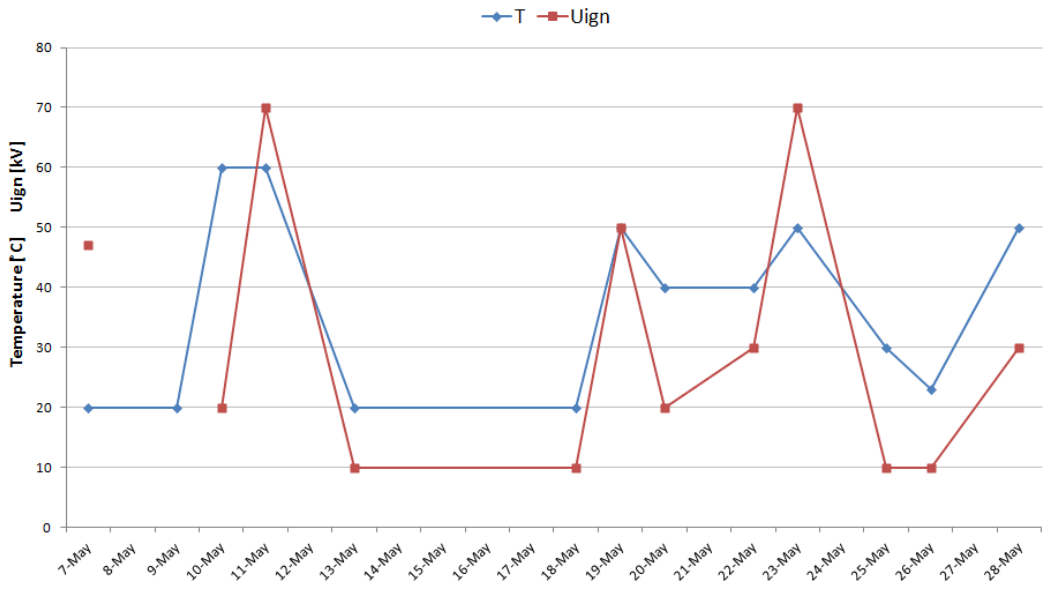

Figure 5.2 – Temperature and applied voltage at discharge initiation.

Although not entirely consistent, a clear correlation between the temperature and the PD inception voltage can be observed in Figure 5.2.

If the same cavity is present at an initially low, then higher temperature, the pressure within the cavity would increase due to the temperature dependent vapor pressure. Based on the Paschen curve in Figure 5.3, one would think that the breakdown voltage of a cavity would decrease with a pressure increase. This is as the height, d, of the butt gap is approximately 0,1 mm and the vapor pressure of clean oils are generally very low, meaning one could assume a placement on the left side of the minimum. The fact that the breakdown voltage increases despite of the likely position to the left of the minimum could imply a change in the geometry. A change in the geometry resulting in increased height of the cavity is however unlikely due to the physical layout of the insulation system. A deeper understanding would be achievable if more information on the gases dissipated in the cavities were at hand. Measurements of the

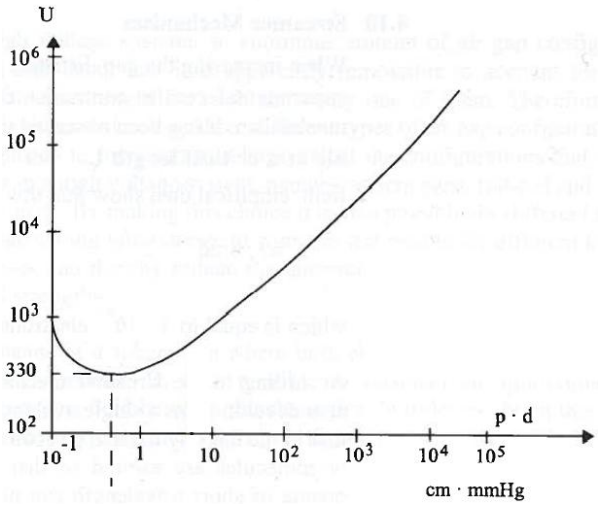

Figure 5.3 – Paschen curve for air [2]

vapor pressure of the cable mass have been considered, but the values are expected to be too low for the instruments and equipment available. [10]

Evenset's research showed that a cavity in a butt gap could grow from the butt gap and continue between the paper layers toward adjacent butt gaps, as shown in Figure 5.4. This would alter the characteristics of the cavity, although still most likely on the left side of the Paschen curve as the thickness of the oil film between the papers is in the μm range. [3]

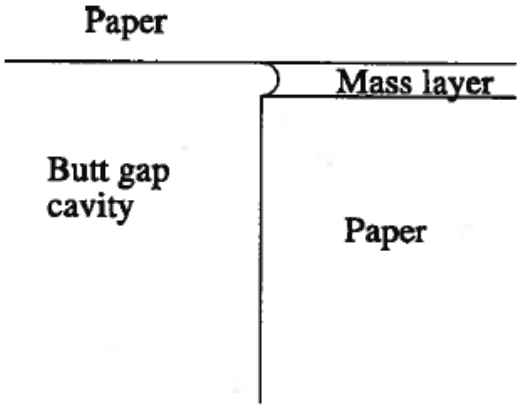

Figure 5.4 – Cavity growth from butt gap into mass layer between papers. [3]

The radial location of a butt gap will also affect the inception voltage due to the field enhancement factor. This could imply that cavities are present close to the conductor at low temperatures and closer to the outer semiconductor at higher temperatures. This would imply radial oil flow.

No correlation between the PD inception voltage and the size of the initial discharges can be derived from these results.

5.3 Discharge site location

To ensure that the measured discharges stem from cavities within the insulation rather than termination problems, a final measurement series to locate the discharges were performed at

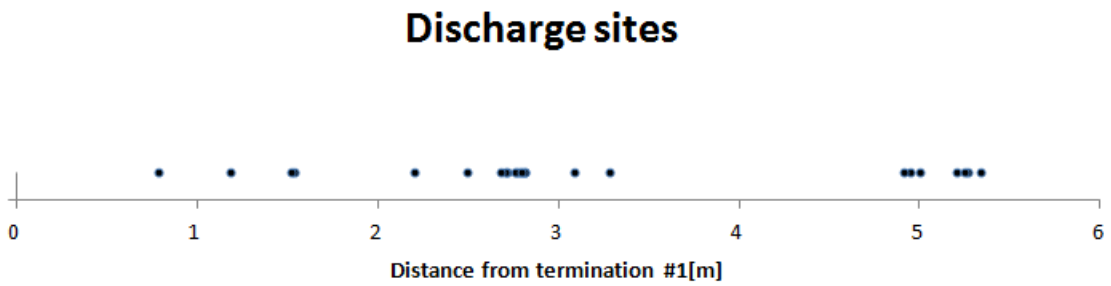

Figure 5.5 – Discharge sites. The discharges seem to be spread evenly along the cable length.

room temperature. This was done by increasing the voltage just above PD inception voltage in order to have a few discharges present. The method shown in Figure 2.6 was utilized.

The discharge sites found are plotted in Figure 5.5. Although difficult to read from this figure, it should be noted that several discharge sites probably were measured multiple times as they appear to be on top of each other. The discharge sites seem to be spread evenly along the length of the cable, not located in the terminations. Some oscilloscope screenshots from these measurements are found in appendix V. As can be seen from the screenshots, the exact times can be difficult to derive due to noise and dampening of the signal through the cable.

5.4 Axial oil flow

The test object should ideally have been an indefinite length of cable to emulate a long subsea cable. In a long subsea cable little to none axial oil transport can occur due to the large internal pressure system, which is why none should occur in the experiments either.

In earlier series of test performed on this cable, less viscous silicone oil was used in the terminations. No discharge activity was detected at voltages below 60 kV, and axial oil flow was suspected due to a lack of anticipated discharges at field levels of approximately 2 kV/mm [8]. In order to reach an electric field of 2 kV/mm close to the conductor, 27 kV has to be applied to this cable, well below 60 kV. The less viscous silicone oil was replaced by the cable mass after tests on a piece of cable confirmed axial flow of silicone oil.

Axial oil flow was not expected to occur in these experiments after the oil change due to the high viscosity of the cable mass, and the fact that the cable ends are raised from the ground to supply an overpressure of approx. 0,2 bar. During the thermal cycling, the oil level in the transparent hoses (Ø=15 mm) at the top of the terminations varied at a visible rate. An oil volume in excess of 100 ml was drained to avoid overflow during heating from room temperature to 60˚C, this was later reintroduced into the bushing during cool-down. Whether or not all the reintroduced oil was absorbed back into the cable is not evident. Because this was unexpected the oil level was not monitored precisely, which in retrospect was a mistake.

6 CONCLUSION

Initially the discharge levels varied with temperature as expected, but this correlation became somewhat unclear mid-test. What caused this change is not evident, as PD's are a stochastic variable affected by several mechanisms. Axial oil flow is however something which should be investigated closely.

One tendency can be observed regarding discharge size; whenever the temperature is changed from one level to a higher level, the size of the largest discharge is reduced. The magnitude of the discharges coincides with values for apparent charge than can be associated with the dimensions of large cavities in partly drained butt gaps.

The inception voltage increases with increasing temperature and decreases with decreasing temperature. No correlation between the inception voltage and size of the discharges at the inception voltage can be derived from these results.

Based on the localization measurements, the home made terminations are performing as intended as the discharge sites were found to be spread evenly along the cable's length and not in the terminations.

6.1 Suggestions for future work

Based on observations made during the lab work some ideas have come to mind regarding the subsequent project work.

- Investigate the phenomenon of axial oil flow by opening one termination on the first test object and doing something in the lines of what is shown in Figure 6.1. With a reservoir in place, heating could be switched on and the oil level monitored.

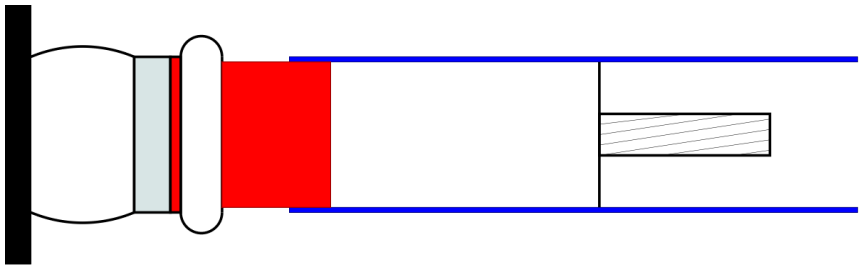

Figure 6.1 – Modification on the termination to check whether there is axial oil flow in the first test object: Large shrink hose (blue) from the silicone tape (red) and out to form a reservoir if mass were to be forced out of the insulation.

- Performing the same measurements as done in this report, but over a larger time span. For example 20→30→40→50→40→30→20℃, one week at each temperature level as the test objects are very large and the time constants likewise.

- Cooling the cable to get a wider temperature specter to confirm/clarify tendencies.

- After the new test object is in working order, a possibly destructive test could be performed on the old test object to investigate the possibility of temporarily overloading the cable. The test object could be heated beyond the recommended maximum continuous conductor temperature by passing current trough the conductor whilst cooling externally to achieve a realistic temperature gradient.

7 BIBLIOGRAPHY

[1] T. Worzyk, “Submarine Power Cables. Design, Installation, Repair, Environmental Aspects”, Springer, 2009.

[2] E. Ildstad, “Electric Power Engineering – TET 4160 High Voltage Insulating Materials”, NTNU, Faculty of Information Technology, Mathematics and Electrical Engineering, Department of Electric Power Engineering, 2010.

[3] G. Evenset, “Cavitation as a Precursor to Breakdown of Mass-Impregnated HVDC Cables”, NTNU Trondheim, Dr. Ing. Avhandling 1999:78, Institutt for elkraftteknikk, 1999.

[4] M. Runde, “Partial Discharge Measurements on NorNed Cables in SINTEF’s Laboratory – Motivation, ideas and procedures” Project memo, SINTEF Energy Research, 2010.

[5] L. Lundgaard, “Partielle Utladninger – Begreper, måleteknikk og mulige anvendelser for tilstandskontroll”, TR A4403, EFI, 1996.

[6] E. Ildstad, ”TET 4195 High Voltage Equipment – Cable Technology”, NTNU, Faculty of Information Technology, Mathematics and Electrical Engineering, Department of Electric Power Engineering, 2009.

[7] Scotch 2220 data sheet, available from: http://multimedia.3m.com/mws/mediawebserver?mwsId=SSSSSu7zK1fslxtUm82UmY_1ev7qe17zHvTSevTSeSSSSSS-- (last accessed 22/5-2012)

[8] M. Runde, “Results from Initial 50 Hz PD Measurements on NorNed Cable Section”, memo, SINTEF Energy Research, 2011.

[9] Private communication with Georg Balog

[10] Private communication with Dag Linhjell

8 APPENDICES

8.1 Appendix I – Oscilloscope screenshots from calibration

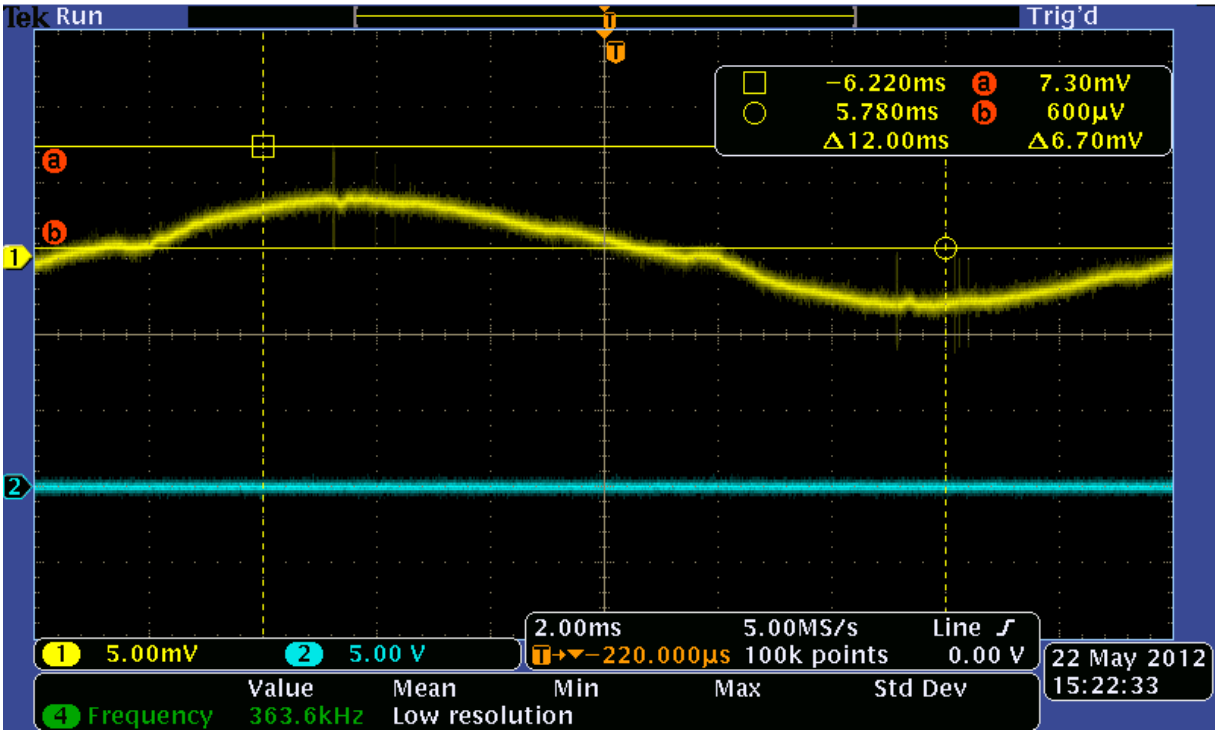

100 pC

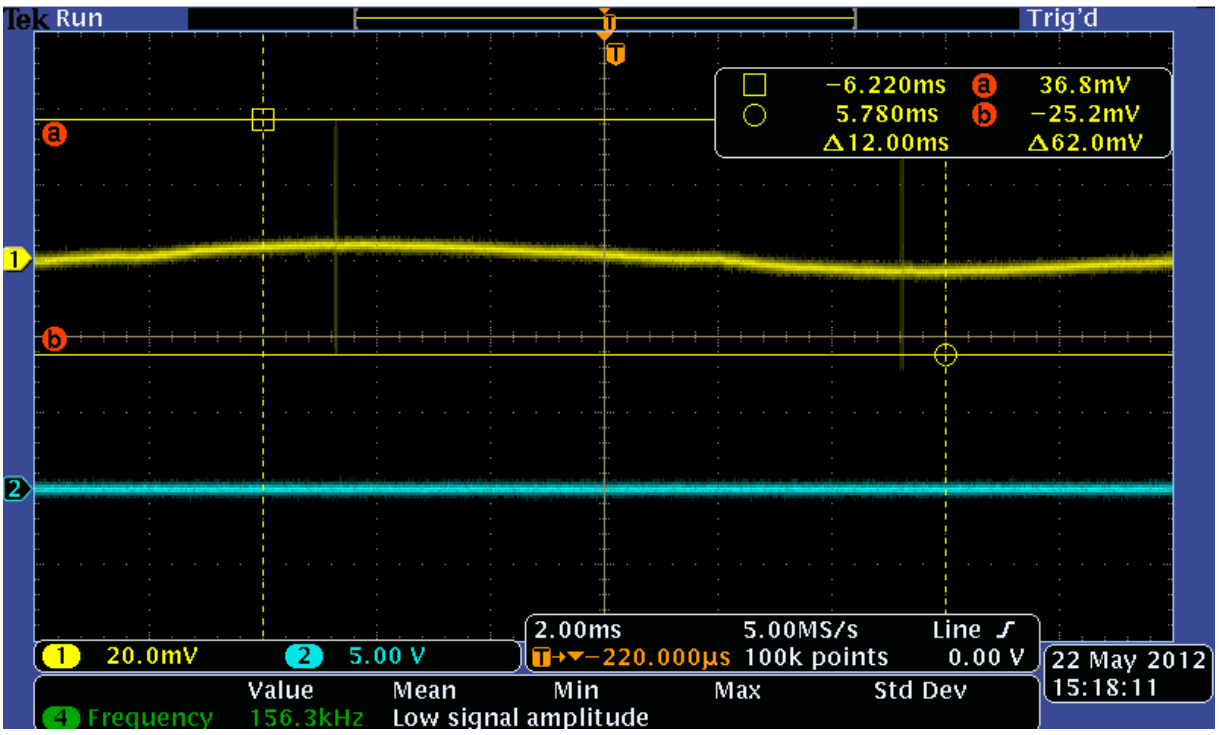

1 000 pC

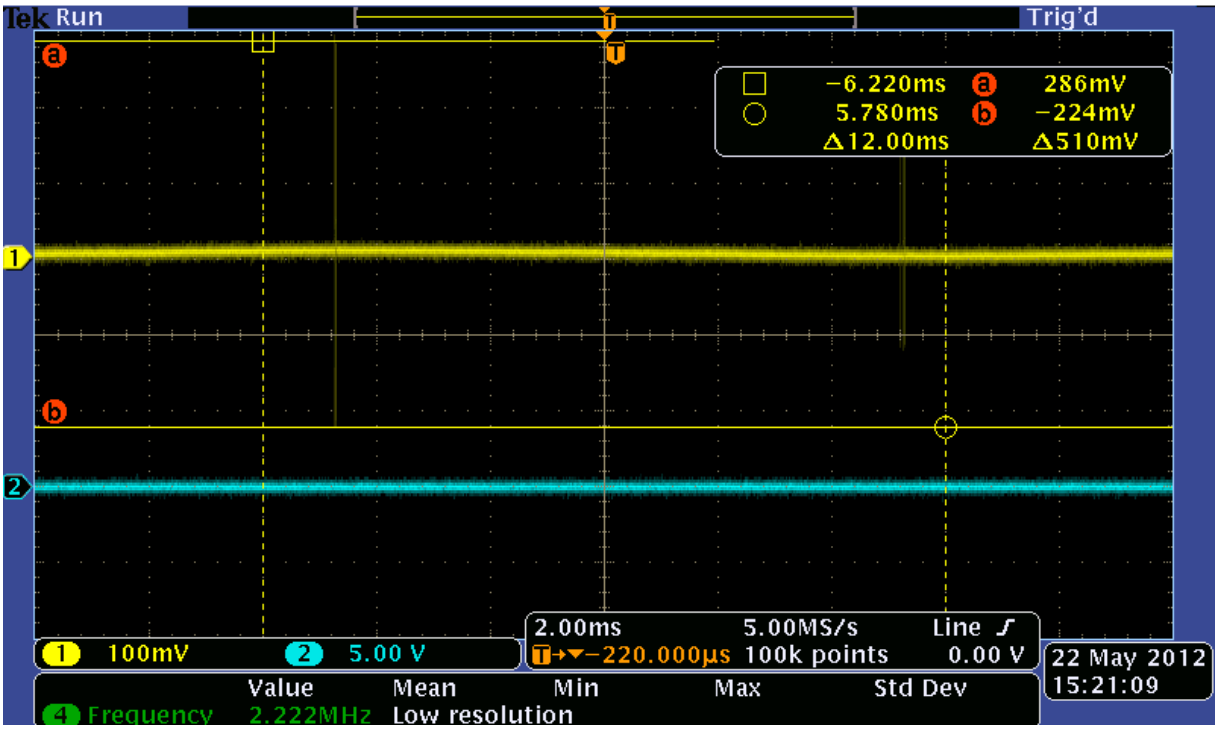
Tek Run
Trig'd
−6.220ms
5.780ms
Δ12.00ms
286mV
−224mV
Δ510mV
100mV
5.00 V
2.00ms
5.00MS/s
Line
−220.000µs
100k points
0.00 V
22 May 2012
15:21:09
Value
Mean
Min
Max
Std Dev
Frequency
2.222MHz
Low resolution

10 000 pC

8.2 Appendix II – Oscilloscope screenshots, ignition- and extinction voltage

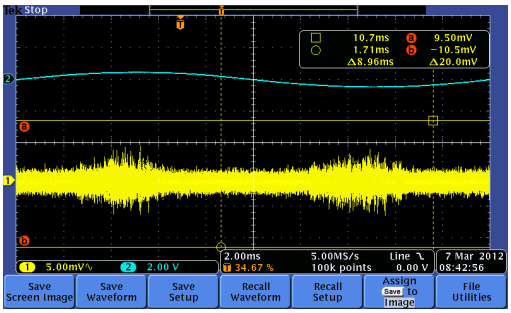

25 kV, 5 pC

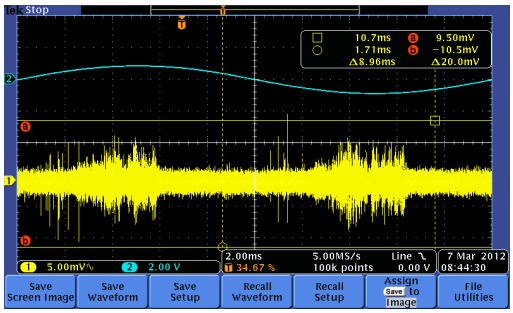

50 kV, 8 pC

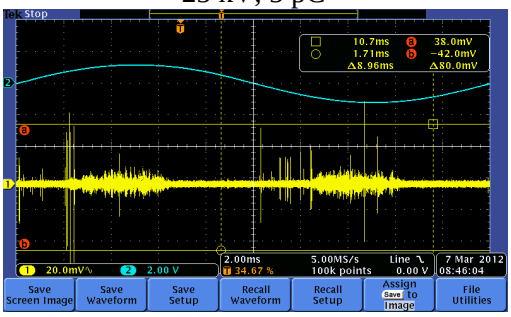

70 kV, 40 pC

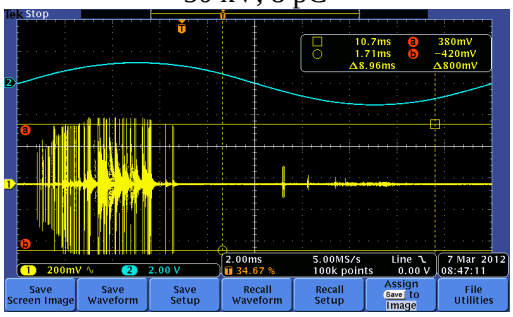

80 kV, 400 pC

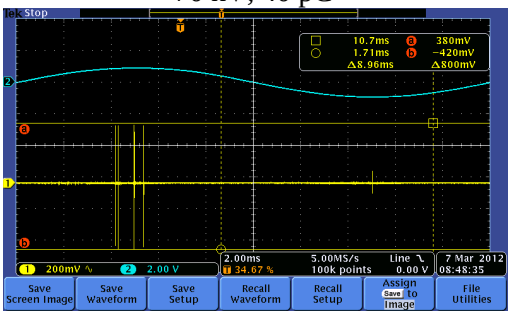

53 kV, 400 pC

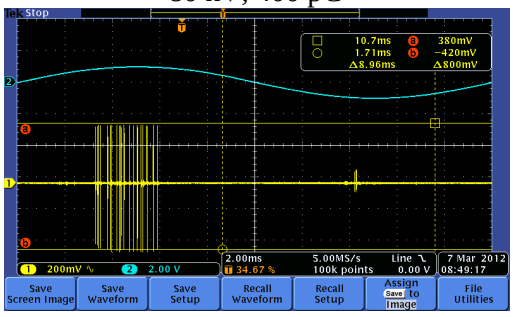

58 kV, 400 pC

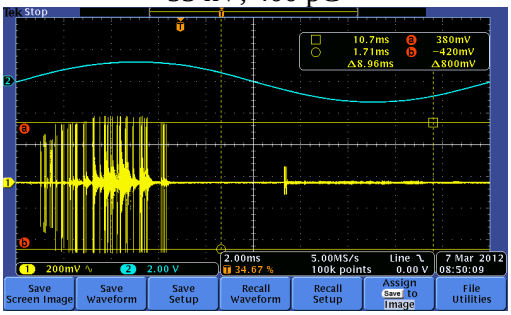

75 kV, 400 pC

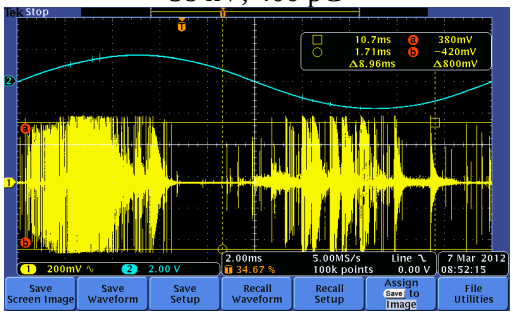

100 kV, 400 pC

8.3 Appendix III – Equipment lists

Equipment set 1:

Description	Registration number
Voltage supply 0-230V	Sintef B01-0756
Oscilloscope, Tektronix TDS 2014B	Elkraft NTNU G04-0349
Calibrator 1-100 pC, Power Diagnostics CAL1A	Elkraft NTNU H02-0171
Measuring impedance, 300 kHz	Elkraft NTNU I6-295
Coupling capacitor, unmarked, 800 pF	
Voltage reference 230/6 VAC	Elkraft NTNU B01-0781
Signal amplifier, Physical Acoustics Corporation	Sintef N07-0106
Voltage supply for amplifier	Elkraft NTNU B02-0430
Filter for separation voltage supply/signal	SEfas N07-0090-01
Filter for supplied voltage, unmarked, 230 V	

Equipment set 2:

Description	Registration number
Voltage supply 0-230V	Sintef B01-0756
Oscilloscope, Tektronix MSO 3014	Elkraft NTNU G04-0365
Calibrator 10-10000 pC, Tettex Instruments	Sintef H02-0090
Measuring impedance, 300 kHz	Elkraft NTNU I6-295
Coupling capacitor, unmarked, 800 pF	
Voltage reference 230/6 VAC	Elkraft NTNU B01-0781
Filter for supplied voltage, unmarked, 230 V	

Equipment set 3:

Description	Registration number
Oscilloscope, Tektronix DPO 5104	Sintef G04-0369
Current probe, Ategam Inc, 93686-1L	EFI I04-0273
Current probe, Ategam Inc, 93686-1L	EFI I04-0274
Filter for supplied voltage, unmarked, 230 V	

8.4 Appendix IV – Oscilloscope screenshots from measurements at each temperature level at 20 kV

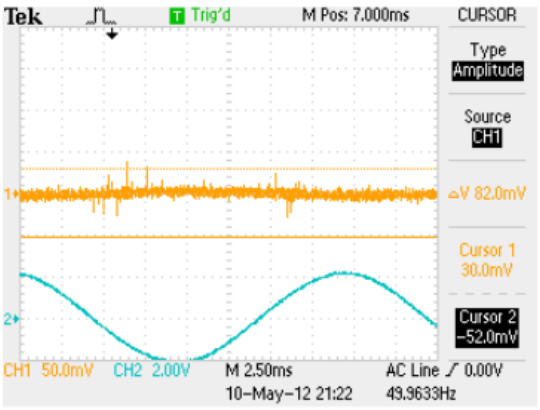

T=60 C, q=8 pC

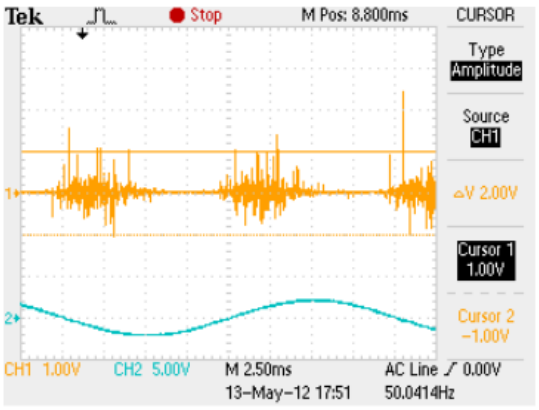

T=20 C, q=471 pC

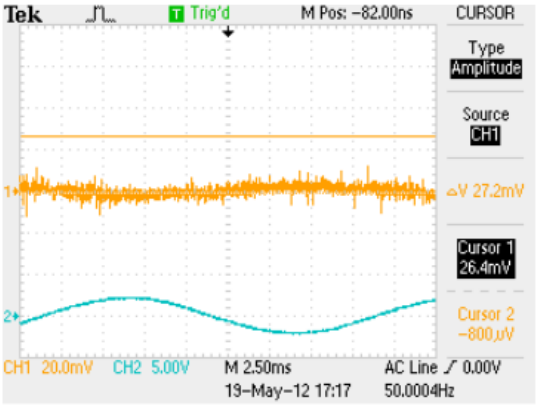

T=50 C, q=less than 2 pC

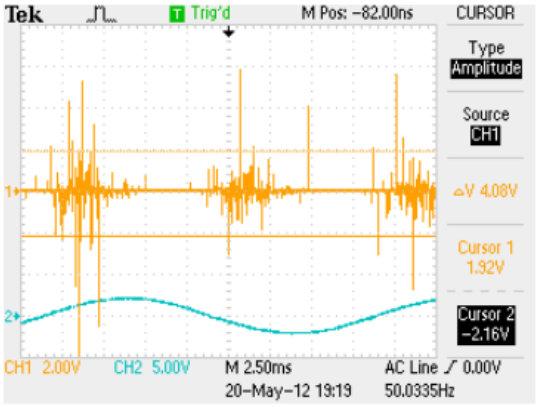

T=40 C, q=784 pC

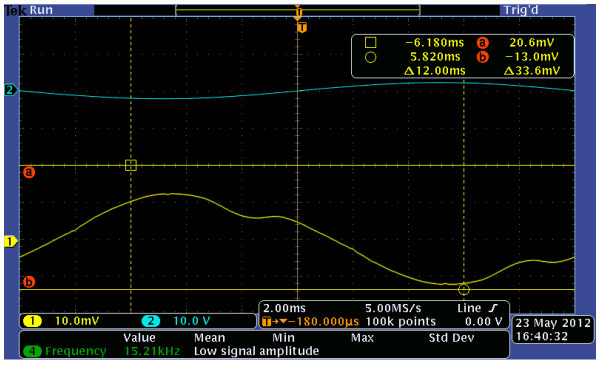

T=50 C, q=less than 100 pC

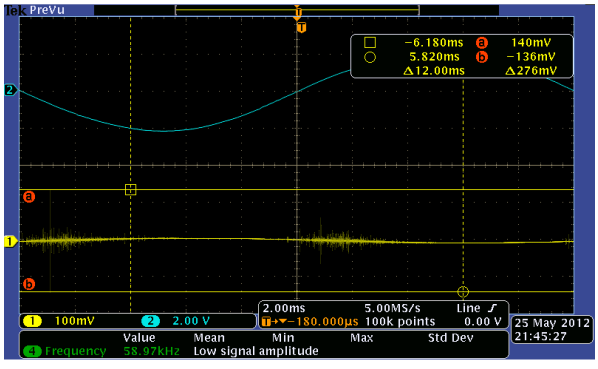

T=30 C, q=4400 pC

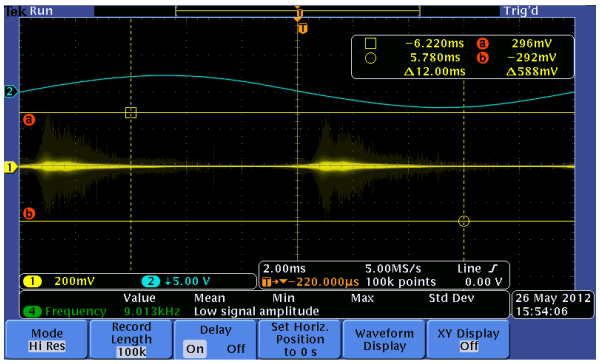

MSO3014 - 10:05:08 26.05.2012

T=23 C, q=9400 pC

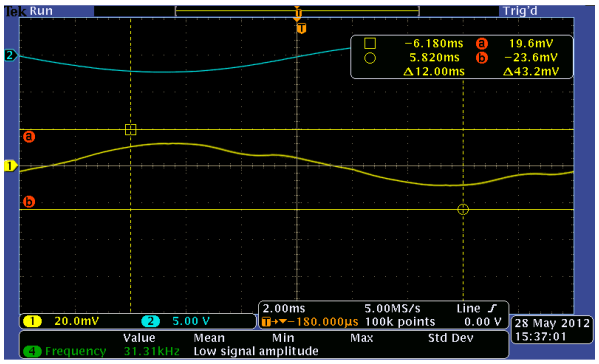

MSO3014 - 09:48:08 28.05.2012

T=50 C, q=less than 100 pC

Calibration for the first four screenshots: 1 pC=10,2 mV

Calibration for the last four screenshots: 1 pC=0,0625 mV

8.5 Appendix V – Oscilloscope screenshots from localization measurements

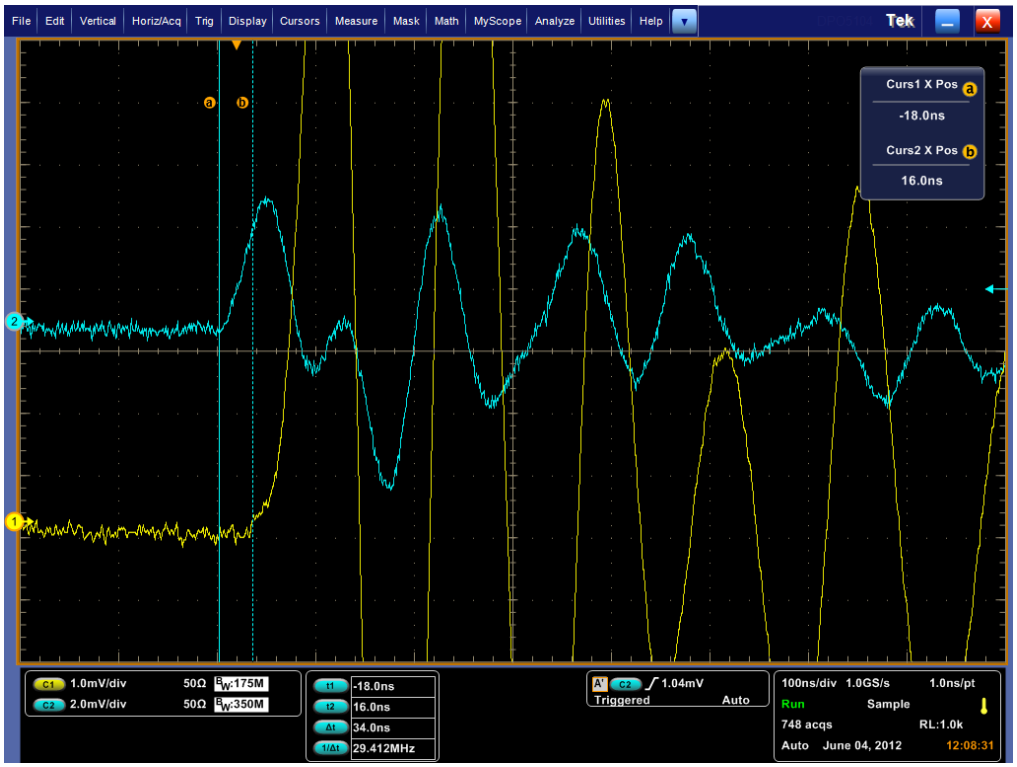

Calibrator at termination #2

Discharge location approx. 1,5 m from termination #1

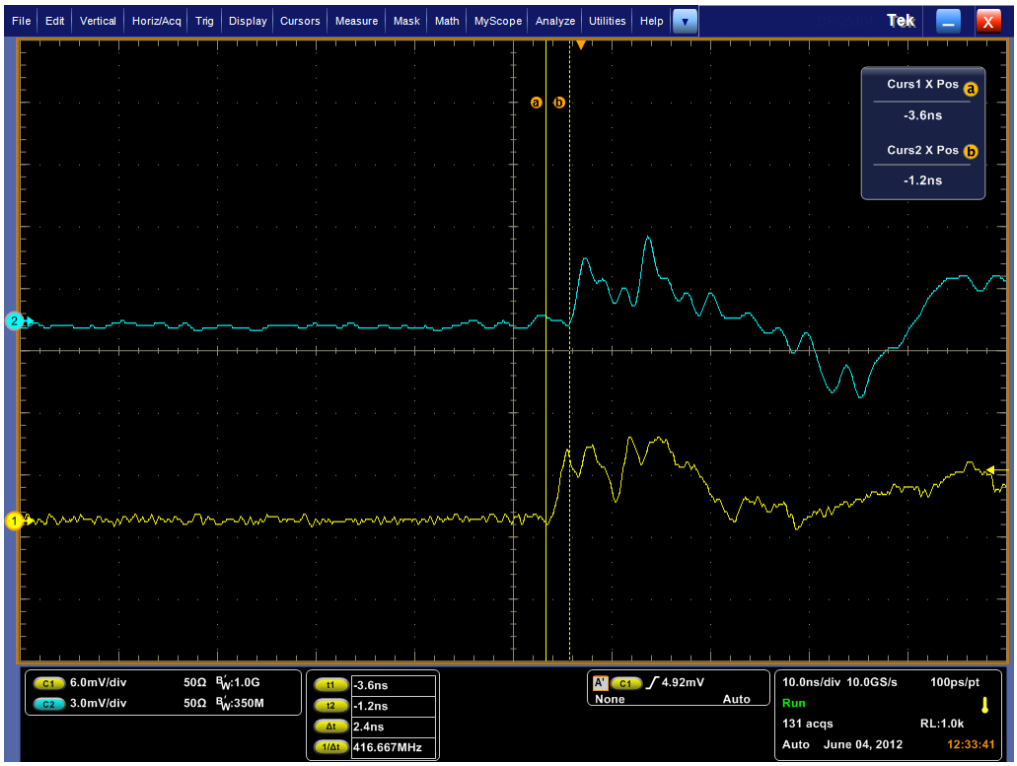

Discharge location approx. 2,8 m from termination #1

Discharge location approx. 1 m from termination #2